

Switchable telescopic contact lens

Eric. J. Tremblay,^{1,2,*} Igor Stamenov,¹ R. Dirk Beer,³ Ashkan Arianpour,¹ and Joseph E. Ford¹

¹*Department of Electrical & Computer Engineering, UCSD, La Jolla, CA 92093, USA*

²*Institute of Microengineering, EPFL, Lausanne 1015, Switzerland*

³*Pacific Science & Engineering Group, San Diego, CA 92121, USA*

*eric.tremblay@epfl.ch

Abstract: We present design and first demonstration of optics for a telescopic contact lens with independent optical paths for switching between normal and magnified vision. The magnified optical path incorporates a telescopic arrangement of positive and negative annular concentric reflectors to achieve 2.8x magnification on the eye, while light passing through a central clear aperture provides unmagnified vision. We present an experimental demonstration of the contact lens mounted on a life-sized optomechanical model eye and, using a pair of modified commercial 3D television glasses, demonstrate electrically operated polarization switching between normal and magnified vision.

©2013 Optical Society of America

OCIS codes: (330.3795) Low-vision optics; (330.4460) Ophthalmic optics and devices; (330.7321) Vision coupled optical systems.

References and links

1. D. S. Friedman, B. J. O'Colmain, and I. Mestrl, "2012 Fifth Edition of Vision Problems in the U.S.," <http://www.visionproblemsus.org/introduction/acknowledgments.html>.
 2. C. Dickinson, *Low Vision: Principles and Practice*, (Butterworth-Heinemann, 1998).
 3. J. P. Szlyk, W. Seiple, D. J. Laderman, R. Kelsch, J. Stelmack, and T. McMahon, "Measuring the Effectiveness of Biotopic Telescopes for Persons with Central Vision Loss," *J. Rehabil. Res. Dev.* **37**, 101-108 (1993).
 4. A. Isen, "Feinbloom miniscope contact lens," *Encyclopedia of contact lens practice*. **13**, 53-55 (1963).
 5. J. Lavinsky, G. Tomasetto, and E. Soares, "Use of a contact lens telescopic system in low vision patients," *Int. J. Rehabil. Res.* **24**, 337-40 (2001).
 6. S. S. Lane and B. D. Kuppermann, "The implantable miniature telescope for macular degeneration," *Curr. Opin. Ophthalmol.* **17**, 94-98 (2006).
 7. E. Peli, "The optical functional advantages of an intraocular low-vision telescope," *Optom. Vision Sci.* **79**, 225-233 (2002).
 8. E. J. Tremblay, R. A. Stack, R. L. Morrison, and J. E. Ford, "Ultrathin cameras using annular folded optics," *Appl. Opt.* **46**, 463-471 (2007).
 9. E. J. Tremblay, R. D. Beer, A. Arianpour, and J. E. Ford, "Telescopic vision contact lens," *Proc. SPIE* **7885**, 788510 (2011).
 10. W. F. Provinces, A. J. Rahe, M. G. Block, T. Pena, and T. J. Tredici, "Yellow lens effects upon visual acquisition performance," *Aviat. Space Env. Med.* **63**, 561-564 (1992).
 11. "HDS HI 1.54™ (pahrifocon A)," http://www.gpspecialists.com/pdf/hsdhi_insert.pdf
 12. R. Watkins, "Zemax Models of the Human Eye," <http://www.radiantzemax.com/kb-en/KnowledgebaseArticle50285.aspx>.
 13. F. W. Campbell and D. G. Green "Optical and retinal factors affecting visual resolution," *J Physiol.* **181**, 576-593 (1965).
 14. R. Hilz and C.R. Cavonius, "Functional organization of the peripheral retina: Sensitivity to periodic stimuli," *Vision Res.* **14**, 1333-1337 (1974).
 15. S. M. Anstis, "A chart demonstrating variations in acuity with retinal position," *Vision Res.* **14**, 589-592 (1974).
 16. A. Arianpour, E. J. Tremblay, I. Stamenov, J. E. Ford, D. J. Schanzlin, and Y. Lo, "An Optomechanical Model Eye for Ophthalmological Refractive Studies," *J. Refract. Surg.* **29**, 126-132 (2013).
-

1. Introduction

Age-related macular degeneration (AMD) is the leading cause of legal blindness for people over 55 in the western world, causing central vision loss in more than 2 million people in the US alone [1]. Individuals with AMD and other degenerative eye disease can use magnifying visual aids to help distinguish details using the functional retina outside of the damaged central fovea. Biotopic telescopes are the most common commercially available visual aids for low-vision [2]. These telescopes are mounted through spectacle lenses at an offset such that the telescope can be brought into view by tilting the head. Biotopic telescopes are useful for some tasks, including driving, but many visually impaired people reject them due to their cosmetic appearance and interference in social interaction [3]. Head-worn approaches also offer only a narrow field of view (FOV) and require that the user turn their head directly towards the viewed scene.

As early as the 1960s, development efforts began on eye-integrated magnification devices such as the Feinbloom “mini-scope” [4], an air-spaced refractive 2x Galilean telescope encapsulated within in a 4.4mm thick contact lens, too thick for sustained use. Hybrid spectacle/contact lens approaches have also been investigated [5], but have not gained acceptance due to poor cosmetics, a limited FOV and vestibular conflict due to the image stabilizing nature of eye movement in the optical system. More recently a fully implantable intraocular miniature telescope (IMT) has become available [6]. The IMT is available in magnifications of 2.2x and 2.7x at $\sim F/12.5$ and includes two small air-spaced glass lenses encased in a plastic lens tube implanted into one of the patient’s eyes in place of the crystalline lens. This solution offers improved appearance and compatibility with social interaction, scanning with eye movement, and a relatively large retinal FOV of $\sim 20^\circ$ (defined by the 50% relative illumination angular field size on the retina) compared to biotopic telescopes [7], but offers limited light collection and requires surgery.

Here we present the design and first experimental demonstration of the optics for a switchable magnifying catadioptric telescope designed to be integrated into a relatively thin (1.17 mm thick) contact lens.

2. Contact lens optical design

Figure 1 shows the optical system, which is based on a concentric multiple-reflection geometry [8,9], designed to provide a combination of telescopic and unmagnified vision through two independent optical paths within a “hard” polymer contact lens structure. The magnified path incorporates a telescopic arrangement of positive and negative optical power to achieve 2.8x magnification on the eye, while a central clear aperture provides unmagnified vision. The dual optical paths make it possible to switch between unmagnified and magnified vision by selective blocking of the central and annular aperture. We have chosen a polarization approach to make the view switchable; using orthogonal polarization films over the apertures combined with a pair of off-the-shelf switching liquid crystal (LC) glasses made for 3D television (Samsung SSG-3100GB).

Figure 1 shows our contact lens design. The contact lens is 8 mm in diameter, 1 mm thick at center, and has a maximum conformal thickness of 1.17 mm at a radius of 1.53mm (see Fig. 1(c)). For such a lens to be comfortably wearable, the overall shape needs to be as conformal as possible to the human eye. This required that we make the annular entrance aperture of the contact positively powered with a curvature approaching that of the eye. Doing so introduces axial chromatic aberration that must be corrected if the full visible spectrum is desired. Alternatively, the spectral bandwidth could be reduced with a photopic color filter [10] to eliminate the need for color correction. However, we chose to design for the full visible spectrum and correct the chromatic aberration using a kinoform diffractive element to maintain color vision. The kinoform was optimized in ZEMAX with a groove depth of 1.13 μm and minimum pitch of 53 μm added to the annular refractive surface. In the wearable lens,

this diffractive element would need to be covered with a smooth contact lens skirt, and the groove depth would be increased to maintain the 1-wave optical phase delay. For example with Polymethyl methacrylate (PMMA) and Paragon Vision Science’s HDS HI 1.54 [11] skirting index, the groove depth would be increased to 11.5 μm .

The current lens is designed in PMMA, a gas-impermeable polymer commonly used for early contact lenses. Modern contact lenses require high levels of gas permeability, and therefore future versions will have to be made from rigid gas permeable (RGP) polymers. We designed the contact lens to provide 2.8x magnification based on a non-gradient index optical human eye model by Rod Watkins [12].

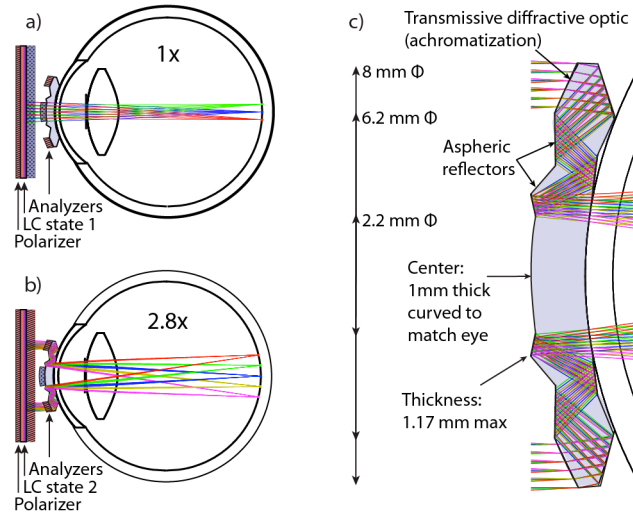


Fig. 1. Optical layout of the magnifying contact lens. (a) Unmagnified (1x) optical path through the central clear aperture of the contact lens. (b) Magnified (2.8x) multiple-reflection path through the contact lens. (c) Expanded view.

3. Modeled performance

Figure 2(a) shows the polychromatic modulation transfer function (MTF) for this optical design (including the optical model of the eye) as a function of object space angular frequency. Several MTF curves are shown in Fig. 2(a) corresponding to object field angles in the tangential (“tan”) and sagittal (“sag”) orientations. The corresponding retinal eccentricity, denoted “e” is also given. Retinal eccentricity is a measure of the field position with respect to the fovea in degrees under normal eye magnification. The suppressed modulation contrast in Fig. 2(a) is a characteristic of diffraction from the annular aperture.

To evaluate the optical benefits of such a telescope we require an estimation of the eye’s contrast threshold across the visual field. A large amount of literature has been written on the contrast sensitivity function (CSF) of the eye, however the majority of these models incorporate the low pass filtering effect of the eye’s optics. For our purposes we require the direct contrast sensitivity of the retina, which is available only from interferometric psychophysical measurement. Our model CSF and contrast thresholds were built from a polynomial fit to detailed foveal data measured by Campbell & Green [13], among others. The CSF outside the fovea was estimated by fitting peripheral threshold measurements of Hilz & Cavonius [14], in combination with an M-scaling approach, to create the estimate of the neural contrast threshold shown in Fig. 2(b). M-scaling has been shown to accurately predict normal, non-interferometric CSF in the periphery where sensitivity is affected primarily by Ganglion cell receptive field size and spacing [15]. The horizontal scale of the contrast threshold in Fig. 2(b) is scaled by the magnification of the contact lens (2.8x). From the

simulated MTF and contrast threshold data shown in Figs. 2(a) and 2(b), we are able to estimate the decimal visual acuity possible with the magnifying contact lens on the eye shown in Fig. 2(c). This suggests that despite the suppressed contrast of the contact lens optics, the contact lens design can provide an increased acuity over $>20^\circ$ retinal FOV ($\sim 7^\circ$ FOV in object space for the magnified view), even for people with normal eye function and full foveal resolution. People suffering from degenerative eye diseases have significantly lower resolution, and so the resolution required of the contact lens optics is correspondingly lower.

In this analysis, we have not included the retinal decenter angle of the fovea – the so-called kappa angle, which is often $4\text{--}8^\circ$ temporally with respect to the optic axis. Because the acuity improvement of the contact lens is limited to a small FOV with best performance coaxial with the contact lens's center axis, the contact lens should ideally be fit to an individual to move the best resolution image away from a patient's scotoma to a region where resolution can be improved through magnification. Regions away from the fovea will have higher modulation thresholds limiting the acuity possible with the contact lens.

The central clear aperture of the contact lens has a diameter of 2.2mm (EFL ≈ 17 mm) giving unmagnified vision with an F-number of 7.8. The outer magnified image has an EFL of 48mm and an effective F-number of 9.4. Figure 2(d) shows the relative illumination (RI) for the magnified path. The 50% RI retinal FOV is dependent on the iris size and varies from approximately $20^\circ\text{--}30^\circ$ for iris sizes of 3mm to 5mm.

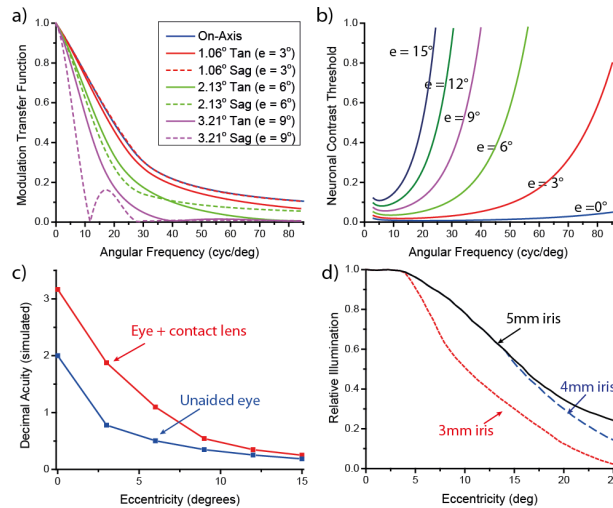


Fig. 2. Simulated optical performance of the 2.8x magnifying contact lens & human eye. (a) Polychromatic modulation transfer function. (b) Estimated neuronal contrast threshold at 2.8x as a function of retinal eccentricity. (c) Decimal Acuity as a function of retinal eccentricity. (d) Relative illumination of the magnified image with varying iris diameter.

4. Fabricated contact lens and optomechanical eye

Figures 3(a) and 3(b) show our first fabricated magnifying contact lens diamond turned by Contour Metrological & Manufacturing, Inc. in PMMA, where the lens's reflective surfaces are turned and coated with patterned aluminum mirrors, then the part is re-chucked and turned to remove the coating over the refractive surfaces. A 1:1 scale (life sized) optomechanical eye was built to fit and test the contact lens onto a corneal surface [9,16] using an index matching gel (1.46 index of refraction). The optomechanical eye shown in Fig. 3(c) consists of two aspheric fused silica lenses (cornea and intraocular) immersed in water. The iris of the optomechanical eye was fixed at a diameter of 4mm. The curved retinal image plane of the eye is achieved using a 10mm diameter fused fiber-optic faceplate with $4.2\ \mu\text{m}$ pitched fibers and

a spherical front face (radius = 22 mm) fabricated by Schott North America. The fiber transfer plate creates a spatial sampling of the image with a Nyquist frequency of 119 cyc/mm. This value is higher than the spatial frequency required for 20/20 vision (1 arcmin, 100 cyc/mm), making the fiber plate suitable for testing resolution up to the 20/20 standard. In terms of angular Nyquist frequency, the fiber plate can support up to 36 cyc/deg (0.84 arcmin) for the unmagnified image, and 100 cyc/deg (0.3 arcmin) for the 2.8x magnified image. The diameter of the curved fiber plate provides a FOV of 34.5°. This is a fraction of the full FOV of human vision, but significantly larger than the $\sim 20^\circ$ FOV of the central retina which includes the macula lutea, and more than sufficient for characterization of the contact lens. Images from the fiber plate were captured by relay imaging the planar rear surface of the fiber bundle through two DSLR lenses in a “front-to-front” configuration onto the CMOS focal plane of a DSLR camera [9]. This image relay system had a variable magnification of 1.4x - 4x. At 4x magnification, the 4.2 μm fibers of the fiber transfer plate could be resolved on the camera, ensuring our ability to measure the resolution of the contact lens and model eye combination.

To electronically switch the contact lens views, a linear polarizer film was placed over the central aperture. This was combined with a pair of Samsung 3D television LC glasses with the rear analyzer removed. The Samsung electronics were also removed and the LC was driven directly with a 200Hz 8V RMS square-wave signal. Figures 3(d) and 3(e) show images of the contact lens and eye through the LC glasses for the two orthogonal polarization states. A polarizing film could also be added to the annular telescopic aperture. We chose to only switch the transmission-state of the unmagnified vision in our experiments so as not to unnecessarily affect the quality of the magnified images.

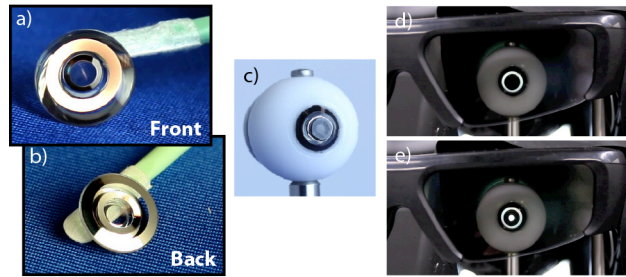


Fig. 3. (a) Contact lens front view. (b) Contact lens back view. (c) Contact lens on optomechanical eye. (d) Central aperture (1x) blocked with LC glasses. (e) Central aperture (1x) open with LC glasses.

5. Performance of the magnifying contact lens

We measured resolution of the contact lens in the laboratory using a USAF 1951 resolution chart. We placed an F/5 36cm lens between the contact lens + eye and the resolution target to enlarge the object conjugate to infinity. Figures 4(a) and 4(b) show images of the resolution chart for the unmagnified (1x) and magnified (2.8x) paths respectively. From Fig. 4(a) we measured a maximum resolution of 1.06 arc minutes (group 2,2) for the unmagnified central aperture of the contact lens. From the magnified image of Fig. 4(b), we observed a lower contrast & lower resolution of 1.34 arc minutes (group 1,6). We believe that the low contrast and poor image quality was caused primarily by the kinoform element, which we measured to have diffraction efficiency below 60% using a rear-projected laser through the contact lens. As discussed in Section 3, mid-spatial frequency contrast is also reduced due to diffraction from the annular aperture. However, previous experience with similarly obscured reflective lenses has shown that image quality and contrast can be subjectively good despite a high obscuration ratio [8,9]. The apparent debris seen in the two images are actually microscopic cracks that developed in the fiber bundle due to prolonged immersion in water.

With the polarizers removed and identical camera settings, the magnified image required an exposure of 4x that of the central aperture to reach saturation. By comparing the F-numbers of the optics we can conclude that we have significant losses in the magnification path, with approximately 40% transmission through the lens. The cascade of four aluminum reflectors account for approximately 34% of the loss ($0.9^4 = 0.66$). The additional losses are due to the inefficient diffractive element. Transmission through the element could be greatly improved by switching to enhanced aluminum coatings (>80% transmission). Figures 4(c), 4(d), and 4(e) show images taken outdoors with the optomechanical eye and contact lens setup. In addition to the large difference in brightness, there is significant contrast masking when both apertures are open simultaneously (Fig. 4(d)). For this reason we do not believe this is a practical configuration and the magnification states should be used one at a time.

Although the magnified images were clearly visible in our tests, acuity fell short of the design specification. To identify the cause, we measured the profile of the contact lens using a Talysurf contact profilometer. Metrology indicated that the contact lens was made with front-to-back decenters of $5 \mu\text{m}$, part thickness error of $3 \mu\text{m}$ and aspheric sag errors $0.5 \mu\text{m}$ – values within our required optical tolerances. We believe that the main source of image quality degradation comes from zero and higher order diffraction from the diffractive kinoform element used to correct chromatic aberration from the first surface curvature.

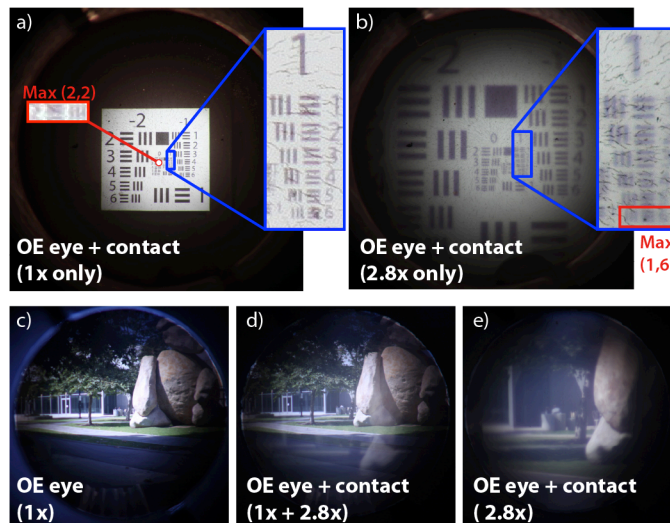


Fig. 4. Images captured through the contact lens and optomechanical eye. (a) USAF resolution chart @ 1x. (b) USAF resolution chart @ 2.8x. (c) Outdoor image taken with optomechanical eye. (d) Outdoor image taken with contact lens and both apertures (1x + 2.8x). (e) Outdoor image taken with contact lens @ 2.8x.

Ongoing research on the telescopic contact lenses will investigate acromatization based on two-material complementary dispersion, rather than a diffractive element. The layout of such an all-refractive contact lens is shown in Fig. 5. This lens is made from the achromatic combination of two RGP polymers made by Paragon Vision Sciences, HDS-100 and HI-1.54. We are also in collaboration to investigate new methods to improve gas permeability, including the incorporation of air-channels into a scleral contact lens structure to remove limitations on material thickness and material permeability. These efforts are the subject of on-going collaborative development, and experimental and clinical test results using this approach will be reported in the future.

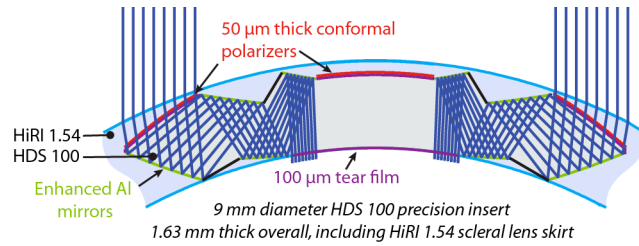


Fig. 5. Initial layout of an all-refractive telescopic contact lens, using two rigid gas permeable polymer materials to correct chromatic aberration without diffractive optics.

6. Conclusion

In summary, we have presented a novel approach to switchable telescopic contact lens based vision, and demonstrated a preliminary prototype magnifying contact lens switching between unmagnified and 2.8x magnified vision measured on a life-sized human eye model. While image quality fell short of design goals, we have identified an all-refractive achromatization approach that offers improved performance, and is the basis of ongoing research.

Acknowledgments

This research was supported by the DARPA SCENICC program under contract W911NF-11-C-0210.

The authors acknowledge Alex Groisman at UCSD for contributing the concept and analysis of air-channel structures for gas-permeability in future contact lens designs.